Geochemical analysis of the WINT-UU-21 core to study volcanism during the Late Triassic (Rhaetian) at Winterswijk

Teun Everwijn 6217036

Supervisors: Bas v.d. Schootbrugge and Remco Bos

Contents

Abstract

The WINT-UU-21 core taken at Winterswijk is studied for evidence of environmental change, specifically volcanism, during the late Triassic and the emplacement of the Central Atlantic Magmatic Province (CAMP). The Late Triassic (Rhaetian) part of the core consists of black shale from 23.985 to 20.2 mbs and red and grey clay (mainly red) until 13.55 mbs. Magnetic susceptibility and carbon isotope data combined with Hg, palaeoproductivity proxies, climatic proxies, and redox proxies are used to determine and compare changes during this time interval with other studies. There is a clear negative Carbon Isotope Excursion (CIE) visible in the $\delta^{13}C$ data, which matches with the Marshi CIE in other studies. Together with Hg data there is a clear indication that there is indeed volcanism taking place during the sedimentation of the core. The volcanism would have taken place in the lowest part of the Rhaetian that is preserved in the core. The Marshi CIE is used to correlate the Winterswijk core to two sites in northern Germany, which also show the extinction interval known as the Triletes Beds above the Marshi CIE. The lithological transition from shale to clay in the core corresponds to the changes from the Contorta Beds (pre-extinction interval) to the Triletes Beds (extinction interval). As there are other Hg spikes in the core without changes in $\delta^{13}C$ it is clear that there is another source of Hg besides volcanism or at least that high Hg concentrations do not mean that there is volcanism taking place. Clear cyclicity likely caused by precession is clearly visible in the Total Organic Carbon (TOC) and climatic proxies used in this study, and slightly less in the magnetic susceptibility. Magnetic susceptibility is not indicative of terrestrial input, as high peaks in the magnetic susceptibility are not accompanied by increases in terrestrial trace elements Fe, Ti and Al. To study palaeoproductivity the enrichment factor of Ba and P are analysed. Both elements are under-enriched compared to the reference shale, but these two elements are not in agreement with each other about the changes in palaeoproductivity through time. This might be due to an outside source of P to the system, as the enrichment factor of P in the extinction interval is not lower than before the extinction interval and anoxia does not seem to play a role in Ba and P recycling. Anoxia is higher in the Contorta Beds than the Triletes Beds, but does not seem to correlate to other changes throughout the core, aside from lower anoxia in the Triletes Beds during drier conditions.

Introduction

There have been five major mass extinctions during the Phanerozoic (Raup & Sepkoski, 1982), at the end of the Ordovician, end of Devonian, end of the Permian, end of the Triassic and at the Cretaceous-Paleogene boundary. The fourth mass extinction occurred at the end of the Triassic (252-201 Ma), starting during the Rhaetian and culminating at the Triassic-Jurassic boundary (Bambach, 2006; Hallam & Wignall, 1999; Kiessling et al., 2007; Raup & Sepkoski, 1982; van de Schootbrugge & Wignall, 2016). In the marine realm 41% of the meso- and microbenthic genera that survived the Norian-Rhaetian boundary became extinct during the Rheatian (Kiessling et al., 2007). In the terrestrial realm forest pollen became less abundant and spores (mainly from ferns) more abundant(Bonis et al., 2009, 2010; Bonis & Kürschner, 2012; Lindström, 2016; Lindström et al., 2019; van de Schootbrugge & Wignall, 2016). Additionally, between 17% and 73% of the Rhaetian pre-extinction palynological flora went extinct (Lindström, 2016).

The Late Triassic and Early Jurassic were marked by widespread volcanism associated with the break-up of Pangea (Lindström et al., 2017, and references therein). Using dating of volcanic ash beds, the Triassic-Jurassic Boundary (TJB) has been dated to 201.36 ± 0.17 Ma (Wotzlaw et al., 2014). The volcanism in the late Triassic and early Jurassic stretches from Europe (Lindström et al., 2017, and references therein) to Brazil (Heimdal et al., 2018) and is called the Central Atlantic Magmatic Province (CAMP). Studies from multiple sites have shown that the eruption of the CAMP and the extensive volcanism were the trigger for the extinction (Lindström et al., 2017).

The effects on the environment and the extinction caused by this volcanism is studied using various proxies. The amount of Organic Matter (OM), usually measured as Total Organic Carbon (TOC), is used to determine changes in palaeoproductivity and preservation of the organic material (e.g. (Lindström et al., 2019; Ruhl et al., 2009)). Total Organic Nitrogen (TON) in combination with TOC is used to determine the C/N ratio that can be used to distinguish changes in organic matter composition (Thornton & McManus, 1994). Stable carbon isotopes, expressed in $\delta^{13}C$, are used to determine the input of volcanism as the $\delta^{13}C$ value becomes lower when there is active volcanism (Bonis & Kürschner, 2012; Lindström, 2016; Lindström et al., 2012, 2017, 2019; Ruhl et al., 2009, 2011; van de Schootbrugge & Wignall, 2016). The $\delta^{13}C$ records over NW Europe reveal distinct negative shifts in $\delta^{13}C$ (Bonis & Kürschner, 2012; Lindström, 2016; Lindström et al., 2012, 2017, 2019; Ruhl et al., 2009, 2011; van de Schootbrugge & Wignall, 2016). Such shifts in $\delta^{13}C$ are called Carbon Isotope Excursions (CIEs), and two major ones are named. The CIE in the Rhaetian is called the “Marshi CIE” and at the TJB is called the “Spelae CIE” (Lindström et al., 2017). In the absence of useful biostratigraphic markers, as is typically the case in mass-extinction events, these CIEs are used as chemostratigraphic markers to correlate different sections and studies together in time. Additionally, mercury (Hg) is presumed to be released during volcanism, and is therefore a good indicator for eruption of the CAMP (Lindström, 2016; Lindström et al., 2017, 2019; van de Schootbrugge & Wignall, 2016).

Volcanism leads to changes in vegetation. This in turn effects runoff into the sea and input of nutrients and trace elements. Palynology is studied for changes in vegetation composition and to understand environmental changes taking place during the extinction via climatic associations of the various palynomorphs. Aside from the loss of taxa mentioned above (Lindström, 2016), there is also a clear spike in spores compared to pollen (Bonis et al., 2009, 2010; Bonis & Kürschner, 2012; Lindström, 2016; Lindström et al., 2017, 2019). Some of these spores are mutated, which shows severe stress on the vegetation and is likely caused by the presence of Hg and therefore volcanism (Lindström et al., 2019).

Other methods to study environmental changes which have been used on late Triassic black shales are some geochemical proxies using trace elements. Barium/Aluminium (Ba/Al) and Phosphorus/Aluminium (P/Al) are used to determine changes in palaeoproductivity, with higher values indicating a higher productivity (Wang et al., 2017). Additionally, two climatic proxies are useful: c-value, which is used to calculate wetness, and Strontium/Copper (Sr/Cu), which is used to determine how dry the climate is. Together they can be used to evaluate climatic changes that are caused by the CAMP. Manganese/Aluminium (Mn/Al) could potentially be used to determine changes in oxygen availability (Tribovillard et al., 2006). Magnetic susceptibility may determine changes in siliciclastic input (da Silva et al., 2013), which has not been used in the studies about the CAMP and the TJB.

Winterswijk is a shallow marine setting close to the CAMP in the Rhaetian (see geological setting), and is therefore a good site to explore the effects of the CAMP on the environment. Although the Winterswijk quarry is famous for its Anisian fossils, such as Nothosaurs and footprints of small reptiles (Oosterink, 1986), not much is known about the Rhaetian in Winterswijk. A palynological study shows that the shales and clays in the Winterswijk quarry are Rhaetian of age (Smeets, 2018). Unfortunately, this study has a low resolution and the concerning data was derived from spudded core samples. Here, I am using a new core that was recently drilled to investigate the Rhaetian in Winterswijk: the WINT-UU-21 core (van Zonneveld, 2021).

This study uses geochemical data to investigate if the CAMP had an influence on this locality and what the environmental changes were during the Rhaetian. The influence of the CAMP is studied by using magnetic susceptibility, carbon measurements (TOC and $\delta^{13}C$), Hg measurements, palaeoproductivity, climatic proxies and tying it all together to volcanism and its effects. Additionally, timing of the Rhaetian within the core is approximated to better link it to other studies. Cyclicity in the data is used to approximate how long it took for the deposition of the Rhaetian part of the core.

Geological setting

During the Triassic the supercontinent Pangea was formed (fig 1.) (Peace et al., 2020) . Pangea was surrounded by the Panthalassa and Tethys Oceans, with Northwestern Europe being covered by a shallow sea. Rift forming via extension around the Atlantic happened during the Middle Triassic (Anisian) in the northern part and Late Triassic (Carnian) in the southern part of the Atlantic. The start of the rifting precedes the CAMP, although generally speaking the breakup of Pangea is contemporaneous with the CAMP (Peace et al., 2020).

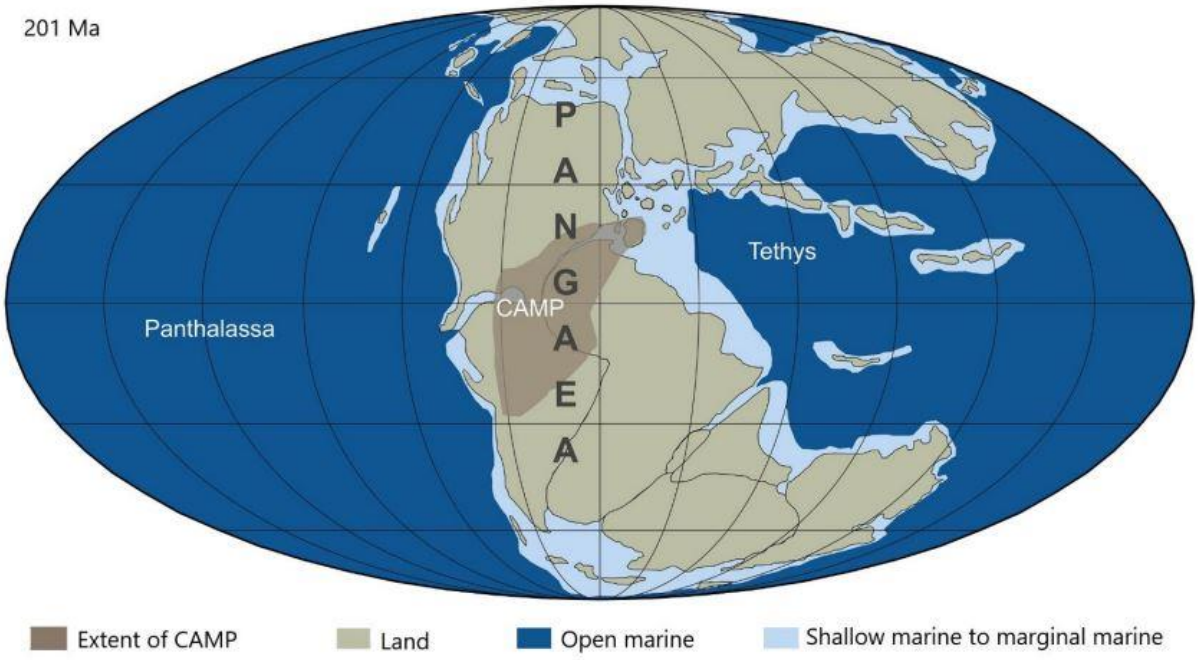

Figure 1. Map of the continental configuration of Pangea and the emplacement of the CAMP. Modified after (Lindström et al., 2021).

The WINT-UU-21 Core (hereafter called “the core”), is taken from Winterswijk, the Netherlands. The core was around the TJB fairly closely located to the CAMP (fig. 2) (Lindström et al., 2017). The distance between Winterswijk and the CAMP emplacement is approximately 550 km. Winterswijk was shallow marine at that time (Smeets, 2018). Changes in the marine ecosystem are directly recorded in the sediment, and changes on land also affect the deposition, due to possible shifts in weathering and erosion that may be caused by climatic changes and changes in vegetation. This influences the amount and type (marine and terrestrial) of organic matter and the trace elements found within the core. Therefore the changes in data reflect environmental changes from both marine and terrestrial sources.

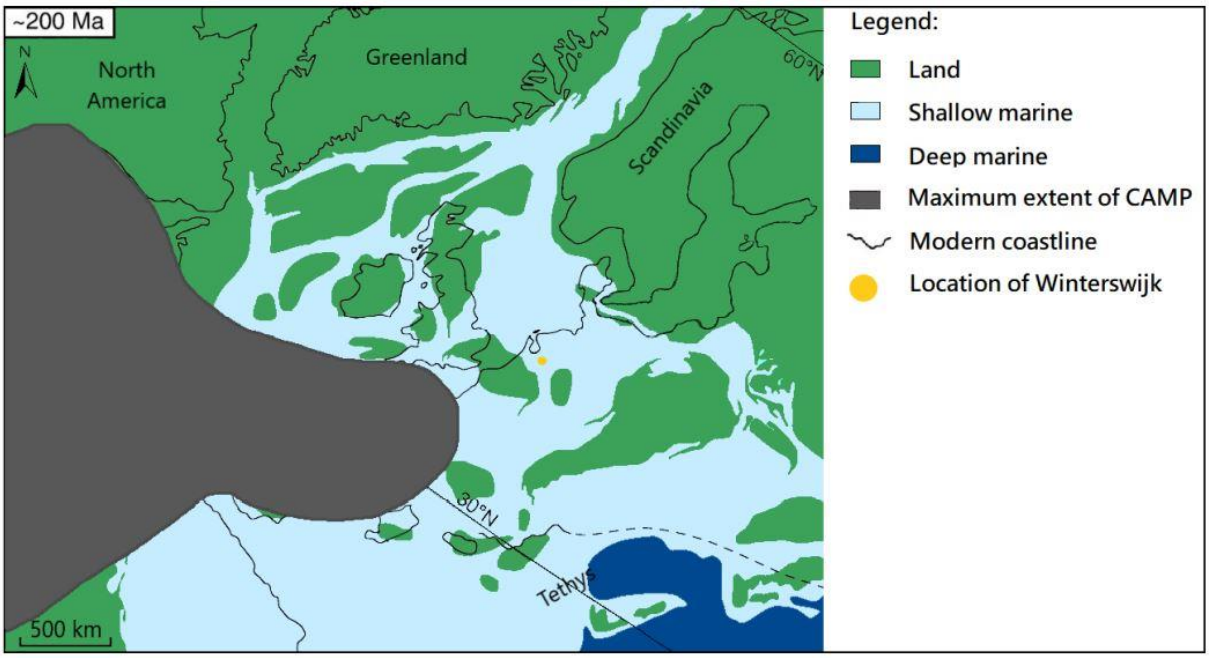

Figure 2. Location of Winterswijk and the Camp around 200 Ma. From (van Zonneveld, 2021)*, modified after* (Lindström et al., 2017).

The Winterswijk quarry is situated in the most eastern part of the Netherlands, close to the border with Germany (fig 3C). The quarry (fig 3A), has had multiple cores taken, and the core from this study is on the northern side of the quarry (fig 3B).

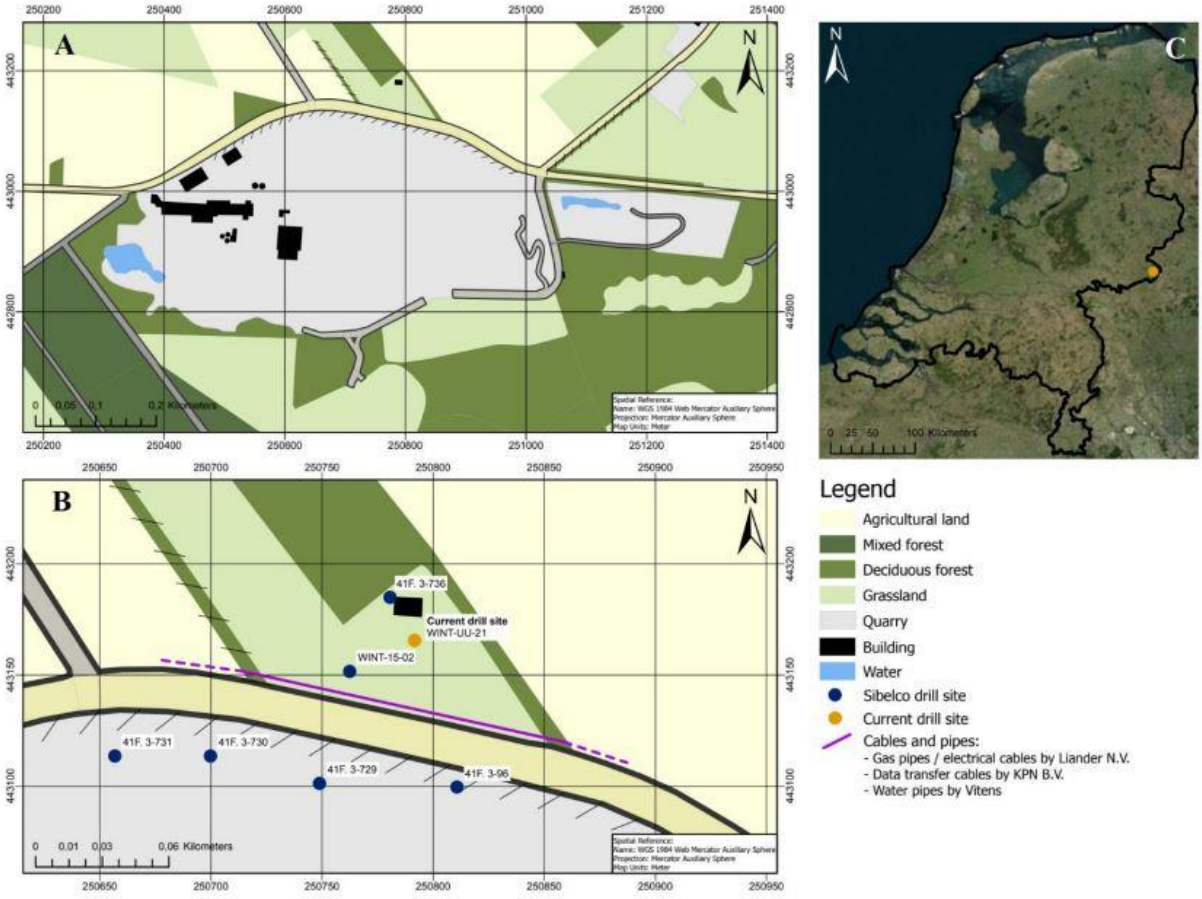

Figure 3. The location of the drilling site, taken from (van Zonneveld, 2021). *(A) Map of the quarry of Winterswijk (Kadaster 2020) (B) An enlargement of the northern wall of the quarry, showing the data provided by the KLIC notification as well as the exact location of the drilling project and preceding drilling projects as documented by Sibelco. (C) Map of the Netherlands, depicting the location of the closest village to the drilling site, Winterswijk (BING 2010).*

The sediments from Winterswijk consist of the Muschelkalk, Rhaetian clays and Early Oligocene clays (Herngreen et al., 2005). The Muschelkalk is deposited during the Anisian (Middle Triassic) and consists of limestone. On top of the Muschelkalk is a few centimetres of clay that is Norian-Rhaetian in age, followed by Rhaetian clays. The Rhaetian clays are topped by Early Oligocene sediments.

The northern wall of the quarry clearly shows distinctive colours (fig 4A) for stratigraphic intervals (fig 4B). These interpretations were made before this study with help of another core taken from Winterswijk (Smeets, 2018).

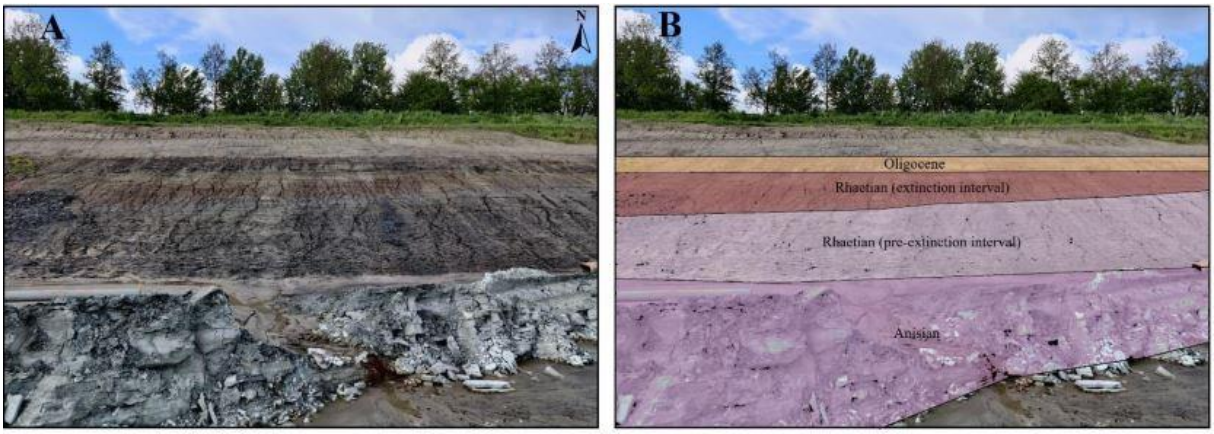

Figure 4. Taken from van Zonneveld, (2021)van Zonneveld, (2021)van Zonneveld, (2021)van Zonneveld, (2021)van Zonneveld, (2021). *Northern wall of the Winterswijk quarry. (A) Clear natural colour pattern distinctive for stratigraphy. (B) Highlighted interpretation of stratigraphy alongside lines that show a change in colour. Picture made in May, 2021.*

The core (fig. 5 and fig. 6) can be divided into five parts: a Quaternary deposit, Oligocene deposit, red and grey clay deposited in the Rhaetian, black shales from the Rhaetian and the Muschelkalk from the Anisian. Due to previous work in Winterswijk, especially a nearby core (Smeets, 2018), the black shales and the red clay are easily identifiable as Rhaetian. The Rhaetian extends from 13.55 to 24 mbs. The lithological shift between the black shales and the red clay in the Rhaetian will be called the transition.

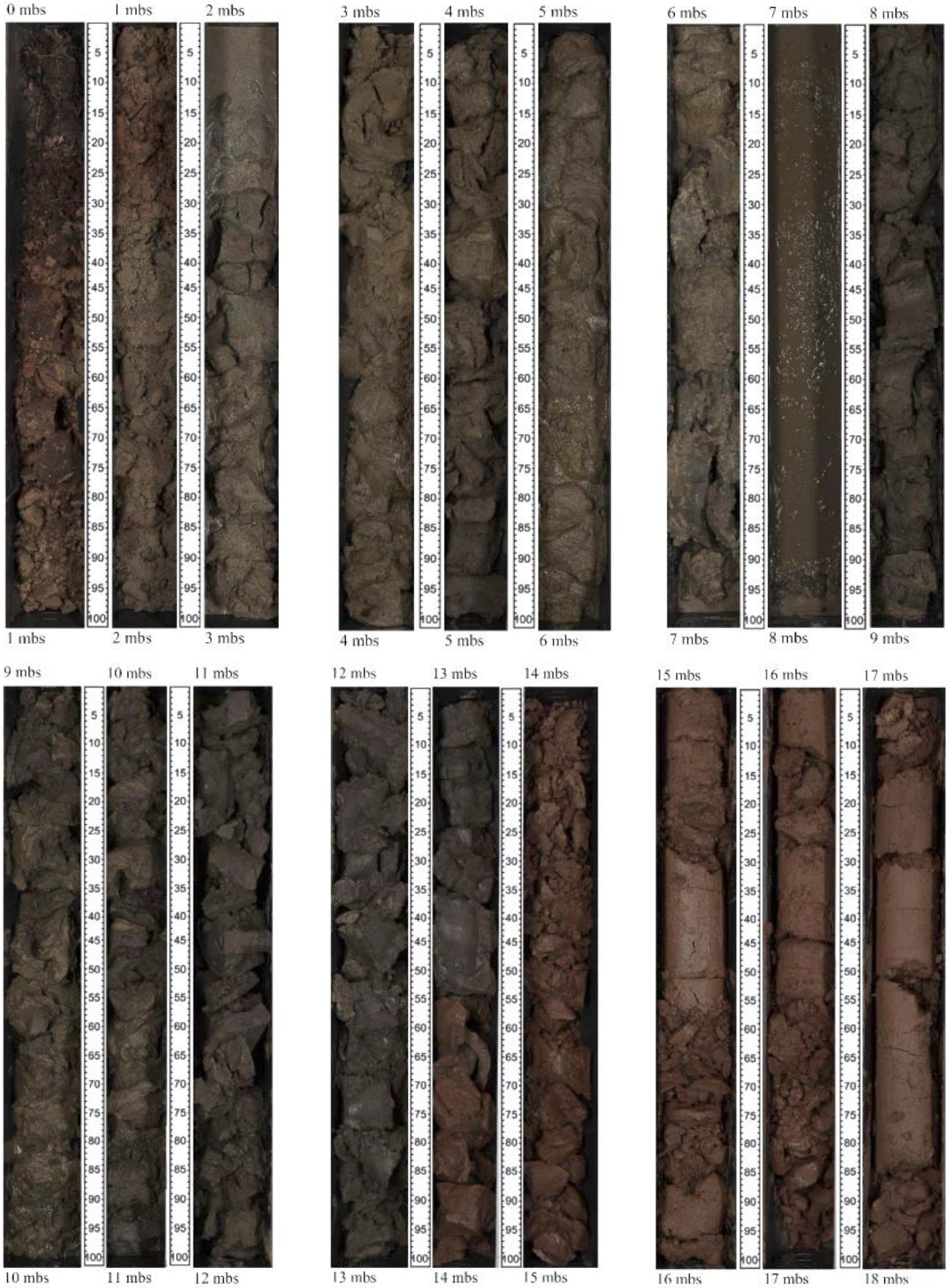
0 mbs
1 mbs
2 mbs
1 mbs
2 mbs
3 mbs
3 mbs
4 mbs
5 mbs
4 mbs
5 mbs
6 mbs
6 mbs
7 mbs
8 mbs
7 mbs
8 mbs
9 mbs
9 mbs
10 mbs
11 mbs
10 mbs
11 mbs
12 mbs
12 mbs
13 mbs
14 mbs
13 mbs
14 mbs
15 mbs
15 mbs
16 mbs
17 mbs
16 mbs
17 mbs
18 mbs

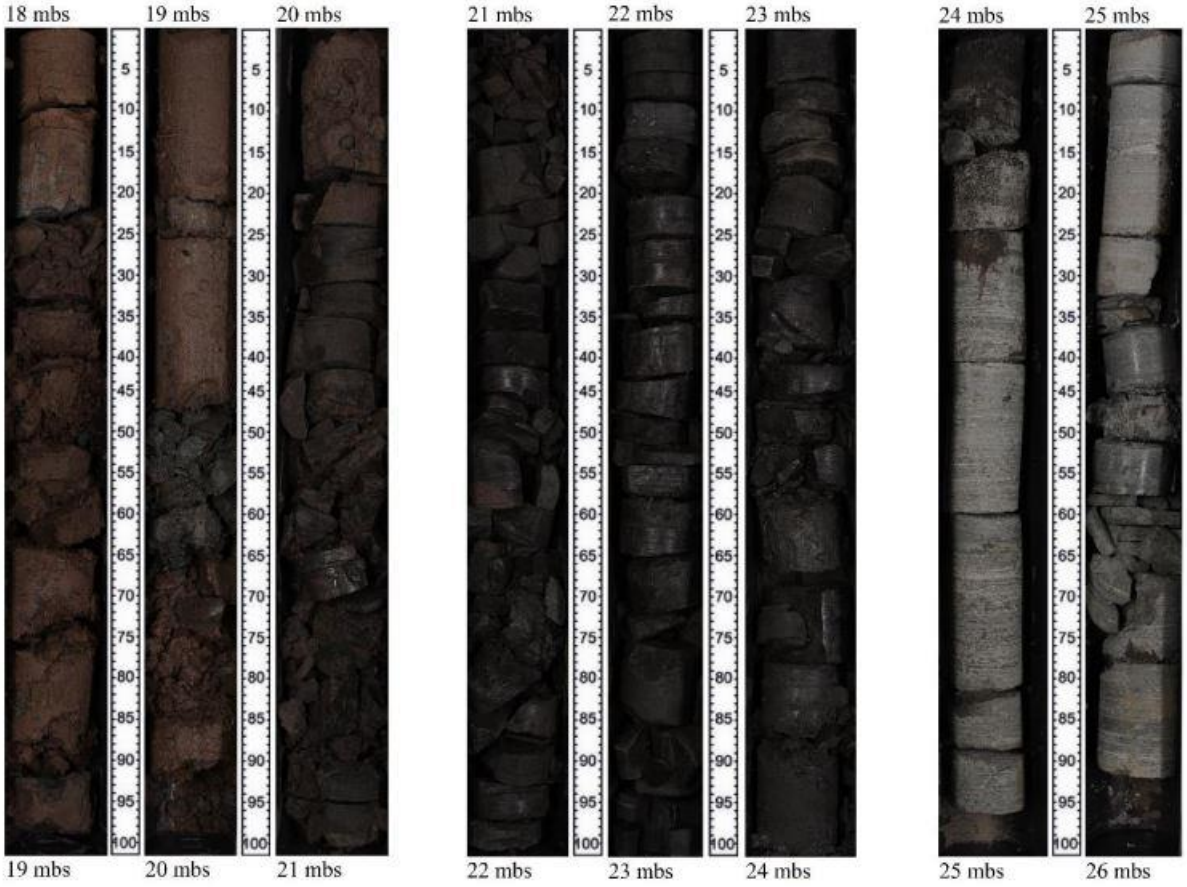

Figure 5. Photos taken from the core from 0-26 mbs.

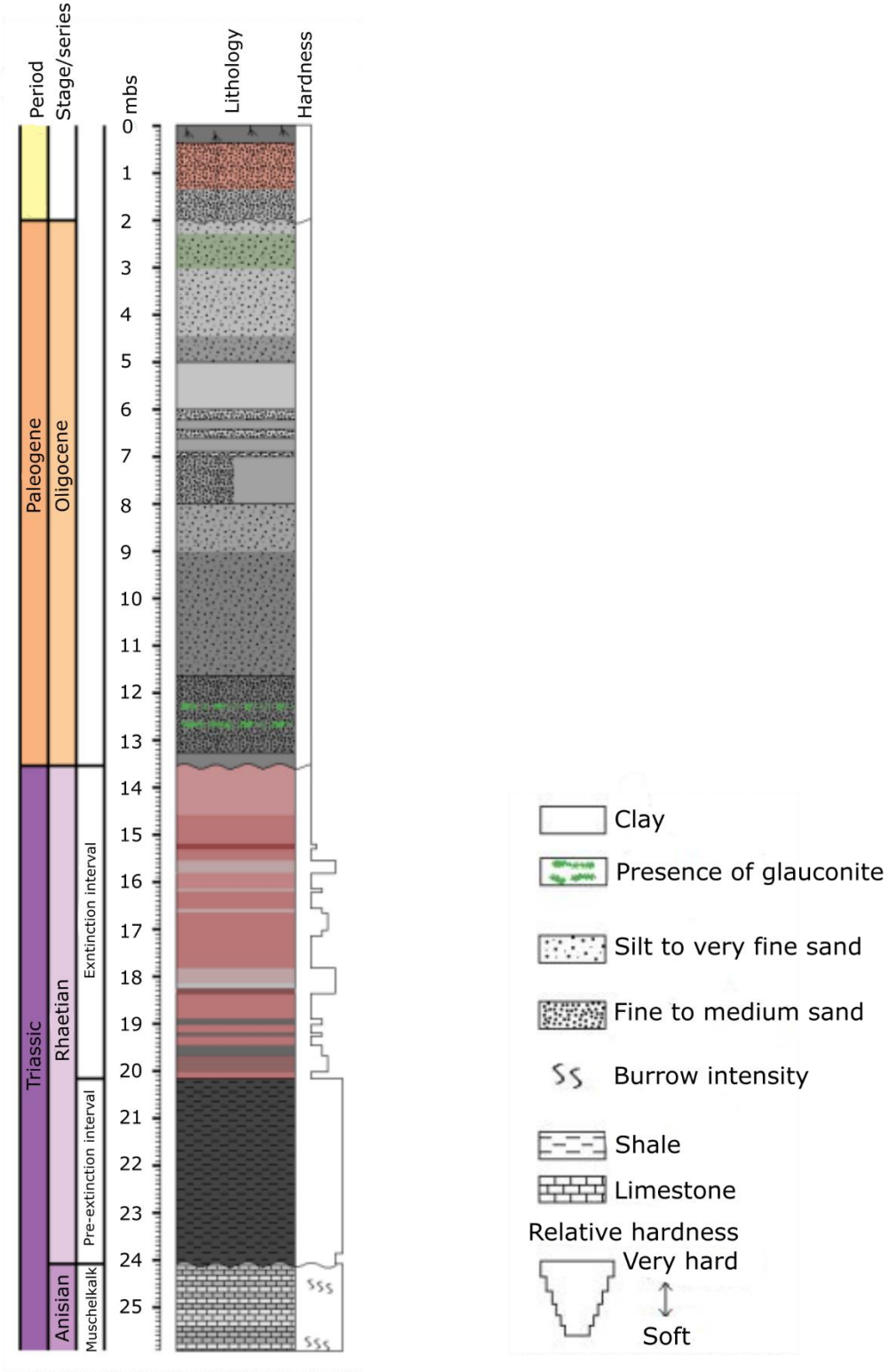

Figure 6. Lithological description of the core.

Methods

Magnetic susceptibility

199 samples were manually crushed and analysed for magnetic susceptibility. The samples are weighed before measuring magnetic susceptibility, as the weight is needed for the machine to calculate the magnetic susceptibility of the sample. The machine is the AGICO MFK1-FA. Calibrating the machine is done by measuring an empty cup at the start of the run. Each sample is at least three times and averaged after that. Some samples had a larger spread and are measured six times. Sample 99 is measured 9 times. Sample 218 is measured first and measured as duplicate multiple times. The measurements are done in Fort Hoofdijk at Utrecht University.

TOC, TON and $\delta^{13}C$

Before TOC, TON and $\delta^{13}C$ measurements the samples were decalcified. 0.3-0.33 g of sample is treated twice with 10 mL HCl and then rinsed twice with 10 mL demiwater. The samples were then dried for 72 hours at 60°C and then weighed. Around 10 mg of sample for the shales were measured for TOC and TON and 25 mg for the clay samples. This is put into a tin cup of 6x12 mm and pressed airtight. Before, after 10 samples and at the end of the measurements an array of standards is used with a blank, nicotinamide 500-1000 μg, acetanilide 200-2000 μg, atropine 200-2000 μg and IVA 15-30 mg. These standards should have a different weight along the measurements to make a calibration curve. The cups are then put into an EA IsoLink IRMS System of Thermo Scientific with a 180 mL/min He flow, a 1020°C oxidation oven and 700°C reduction oven. To calculate TOC and TON a correction is made for the partial loss of organic matter with decalcification.

With $\delta^{13}C$ the weight of the sample should be 30 μg of carbon, with an error margin of 10%. The cups are 5x9 mm. The standards used are a blank, Nicotinamide 50-100 μg and GQ of 1500-3500 μg. The same instrument is used.

All the measurements are done at the Geolab on the fifth floor of the VMB at Utrecht University.

Hg

A total 114 sediment samples were subjected to bulk mercury (Hg) measurements. Approximately 150 mg of powdered sediment were placed in a glass holder before being transferred in a Spectronic combustion chamber. The samples were subjected to ~600 degrees Celsius, after which all mercury retained within the sample volatized and were

measured using a RA-915+ Zeeman Mercury Spectrometer. Quantification of the measurements was achieved through the measurement of the 290-paint standard (paint chips) with an accepted value of 290 ng/g Hg. Accuracy and precision were determined at 10.04 ng/g and 4.97 ng/g, respectively. Repeated standard measurements of different weights resulted in a linear regression with a slope of 1.6691. By multiplying the accepted slope with the ratio of area intensity over weighed a bulk concentration of Hg which are reported as ng/g sediment (i.e. part per billion (ppb)). The Hg measurements were done at Oxford University.

ICP-OES

The ICP-OES data is generated by total destruction. The acids used in the destruction are 48% HF, 72% HClO4, 65% HNO3 and 30% HCl. From this the following acids are made: mixed ($HClO_4$:HNO_3=3:2), 4.5% HNO_3 and 4.5% HCl. The procedure for ICP-OES measurements is as follows: measure the weight of an empty Teflon vial and add 125 mg sample. For my measurements 2 blancos, 2 standards and 4 duplicates are measured alongside the samples. To each sample is 2.5 mL mixed acid and 2.5 mL HF is added and then mixed. The vials are then 1 night put in an aluminium holder at 90°C. Let them cool down to room temperature before placing them back at 160°C. Evaporate the samples until there is a gel-like substance at the bottom of each vial. Add 25 mL 4.5% HNO_3 to each vial and place them at least 2 hours in the aluminium holder at 90°C. Wait until the vials are cooled down to measure the dilution.

The ICP-OES data is measured using Perkin-Elmer Avio 500 ICP-OES instrument and the plasma is looked at radially. The plasma gas is Ar 10 L/min, nebuliser gas Ar 0.075 L/min, auxiliary gas Ar 0.2 L/min, the shear gas is N_2 25 L/min and the peristaltic pump is 1.5 ml/min. RF generator is set on 1500 watt. This machine has only 2 detectors and is not completely simultaneous. It has a range of 163-782 nm.

The measurements are done at the Geolab on the first floor of the VMB at Utrecht University.

Enrichment Factors (EF)

Enrichment Factors (EF) are used to determine if a sample is enriched in a certain element compared to a standard (reference) shale. The standard shale used is taken from (Turekian & Wedephol, 1961). There are two ways to calculate the EF: ratio of the element in the sample and the reference shale (Lee et al., 1998) or the ratio between the element and aluminium in the sample divided by the ration between the element and aluminium in the reference shale (Tribovillard et al., 2006). An EF of 1 means there is no enrichment, below 1 is depleted and above 1 is enriched compared to the reference shale.

Acycle

For determining cyclicity in the TOC in the shale and magnetic susceptibility in the clay the program Acycle is used (Li et al., 2019). The data is resampled with a sampling rate of 1 sample every 0.1 m for the TOC and 1 sample every 0.05 m for the magnetic susceptibility. The magnetic susceptibility is also rLOESS detrended. Afterwards, filters were made with frequencies 0.43243-0.64865 for the TOC and 1.28-1.59 for the magnetic susceptibility.

Results

Carbon and nitrogen measurements

The $\delta^{13}C$, TOC and C/N ratio reveal information about changes in organic matter over time (Schobben et al., 2019; Thornton & McManus, 1994). Additionally, $\delta^{13}C$ is also influenced by atmospheric processes and changes in $\delta^{13}C$ in the atmosphere (Lindström et al., 2019, 2021; Ruhl et al., 2011). Changes in the $\delta^{13}C$, TOC and C/N ratio through time (fig. 7), show that $\delta^{13}C$ decreases when TOC and C/N increases, and that TOC and C/N increase simultaneously. A more detailed look at the data shows that in the marl $\delta^{13}C$ shows an increase in $\delta^{13}C$ to -25.56‰, after which the isotope value lowers to an absolute minimum of -28.55‰ at 23.72 mbs in the shale. At the same time the TOC and C/N values increase, signifying an increase in organic matter. The same relationship between $\delta^{13}C$, TOC and C/N is visible at 22.78 mbs, although the negative shift in $\delta^{13}C$ is much smaller. However, $\delta^{13}C$ shows less variability afterwards compared to TOC and C/N. This would indicate that the negative $\delta^{13}C$ spike around 23.72 mbs is different from other negative shifts in magnitude and duration of the shift. The first shift towards the absolute minimum is likely a Carbon Isotope Excursion (CIE), as the magnitude of change is higher than that of other shifts in $\delta^{13}C$. The transition is characterised by a large shift towards more positive values for $\delta^{13}C$, and a negative shift for TOC and C/N. The clay shows less variability than the shale, with no large negative shifts in $\delta^{13}C$ visible, very low TOC content and little change in C/N.

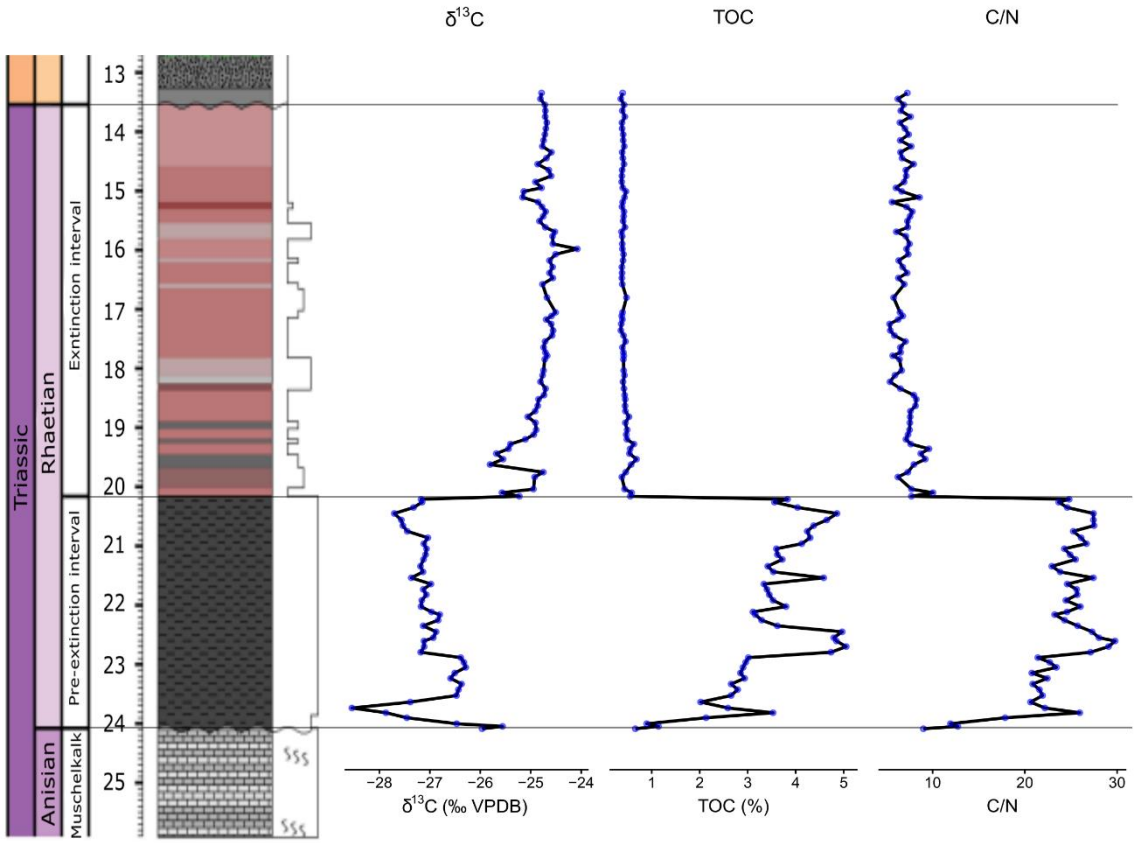

Figure 7. Carbon measurements (δ¹³C, TOC and C/N ratio) plotted next to the core.

δ¹³C correlation

As there is a CIE in the lowest part of the core, δ¹³C can be used to correlate different cores and sections to each other. Using the Schandelah core (Lindström et al., 2017; van de Schootbrugge et al., 2019) and the Bonenburg section (Gravendyck et al., 2020; Schobben et al., 2019), a timeline of environmental changes can be made. As is visible in figure 8, both Schandelah and Bonenburg show a CIE. There are two main CIEs in the Rhaetian, the Marshi CIE and the Spelae CIE, which characterises the TJB, although the Spelae CIE at the Bonenburg section happens before the TJB. As the TJB is not visible in the core, the CIE at Winterswijk is clearly the Marshi CIE and can therefore be correlated to the Marshi CIE at Schandelah and Bonenburg. The Marshi CIE at Schandelah has already been determined by Lindström et al. (2017), but Bonenburg does not use the same terminology. Due to changes in palynology (Gravendyck et al., 2020) and the amplitude and order of the δ¹³C changes greatly resemble those at Winterswijk the first of two negative δ¹³C spikes is likely to be the Marshi CIE. A second tie point is the change from the pre-extinction interval to the extinction interval. The pre-extinction interval is defined as the Contorta Beds, and the extinction interval as the Triletes Beds. This has already been studied for Schandelah and Bonenburg, and the lithological shift in the core combined with an increase in δ¹³C is similar to the

transition from the Contorta Beds to the Triletes Beds in Bonenburg. Combined with the fact that the clay is already known as the extinction interval it is clear that the shale forms the Contorta Beds and the clay the Triletes Beds.

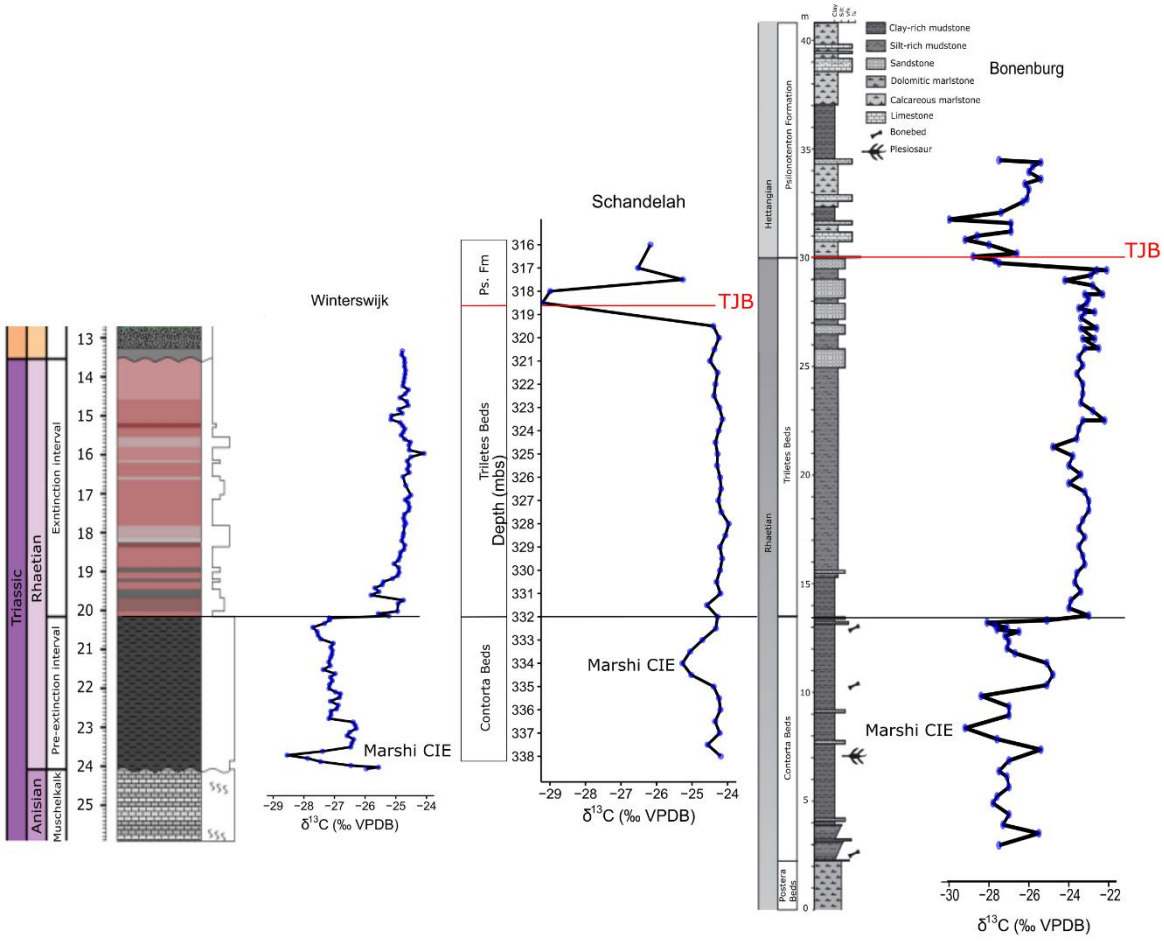

Figure 8. δ¹³C curves and stratigraphy of the core, the Schandelah core (Lindström et al., 2017; van de Schootbrugge et al., 2019)*and the Bonenburg section* (Gravendyck et al., 2020; Schobben et al., 2019).

Enrichment factors

The enrichment factors of the measured elements are plotted for two different samples to see the effect of the different calculations for the Enrichment Factor (see methods) and to see the difference between shale and clay (fig. 9). These samples have no spike in the other data from this study and as such can be seen as part of general background conditions. For all elements, the enrichment factors from Lee et al. (1998) are higher than Tribovillard et al. (2006), due to Tribovillard et al. (2006) using Aluminium (Al) in their calculation and there is a higher Al content in the core compared to the reference shale. One element is clearly more enriched than the others, which is sulphur (S) in the Contorta Beds (fig. 9), but, S is depleted in the

clay. The high enrichment factor of S in the shale is likely due to pyrite, as pyrite is visible in many shale samples, even though there is no pyrite directly visible in the sample from 21.63 mbs. Other notable enriched elements are Lithium (Li) and Scandium (Sc). Quite a few elements are depleted in both the Contorta and Triletes Beds: Natrium (Na), Phosphor (P), Manganese (Mn), Zinc (Zn), Strontium (Sr) and Barium (Ba).

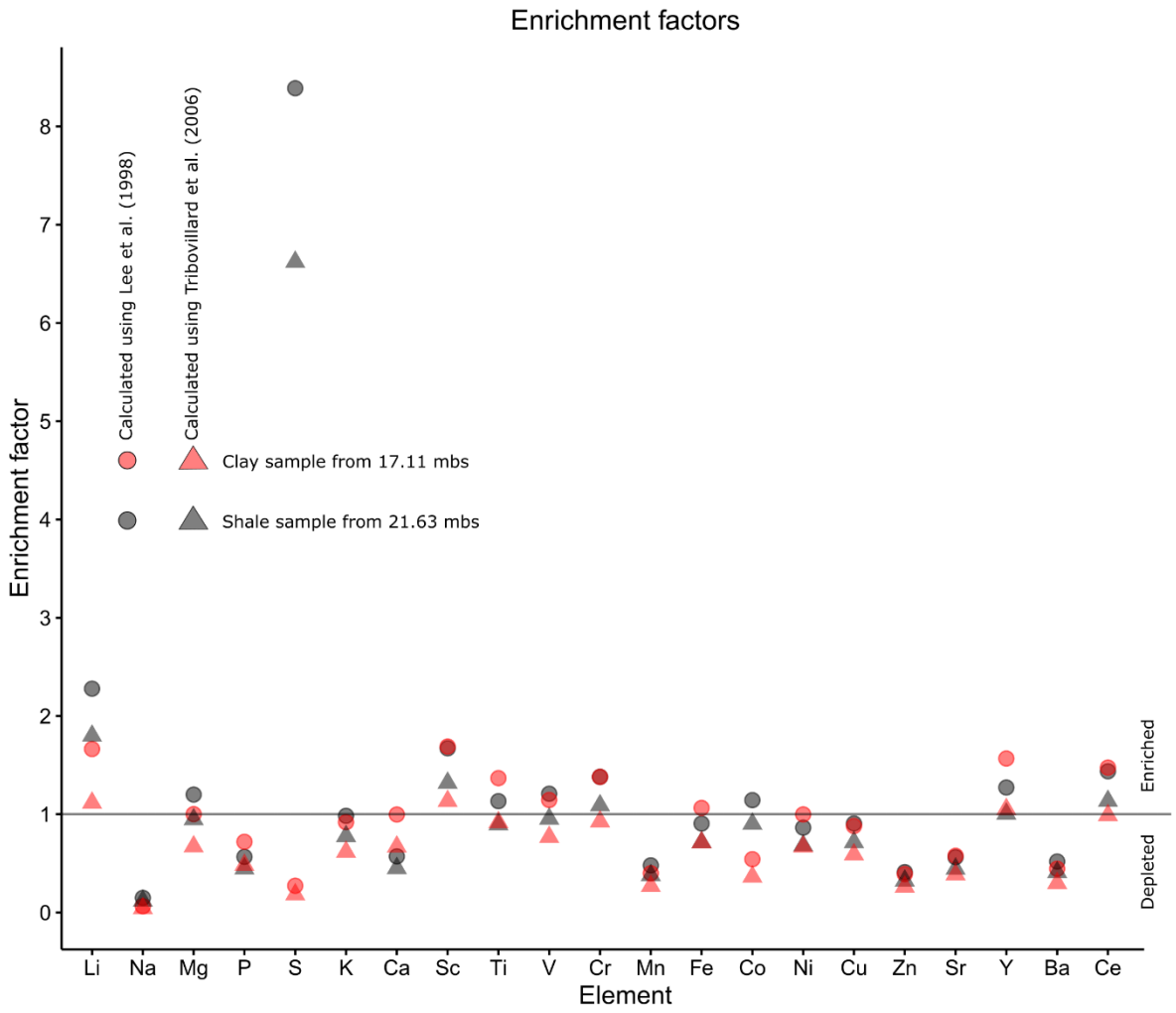

Figure 9. Enrichment factors of the measured elements sorted by atomic number.

Magnetic susceptibility

Magnetic susceptibility in the Contorta Beds shows very little variability (fig. 10). A large peak is observed at the transition, with a value of 4.43e-7. The magnetic susceptibility stays high until 19.825 mbs where the magnetic susceptibility has a value of 7.79e-8. After the transition the magnetic susceptibility shows a large amount of variability with two high peaks in the average kappa, 1.95e-7 at 17.11 mbs and 3.41e-7 at 15.11 mbs. When comparing the magnetic susceptibility data to the EF of Fe and Ti and the absolute concentration of Al, there seems to be no match between changes in magnetic susceptibility or elements that are mainly derived from weathering and erosion.

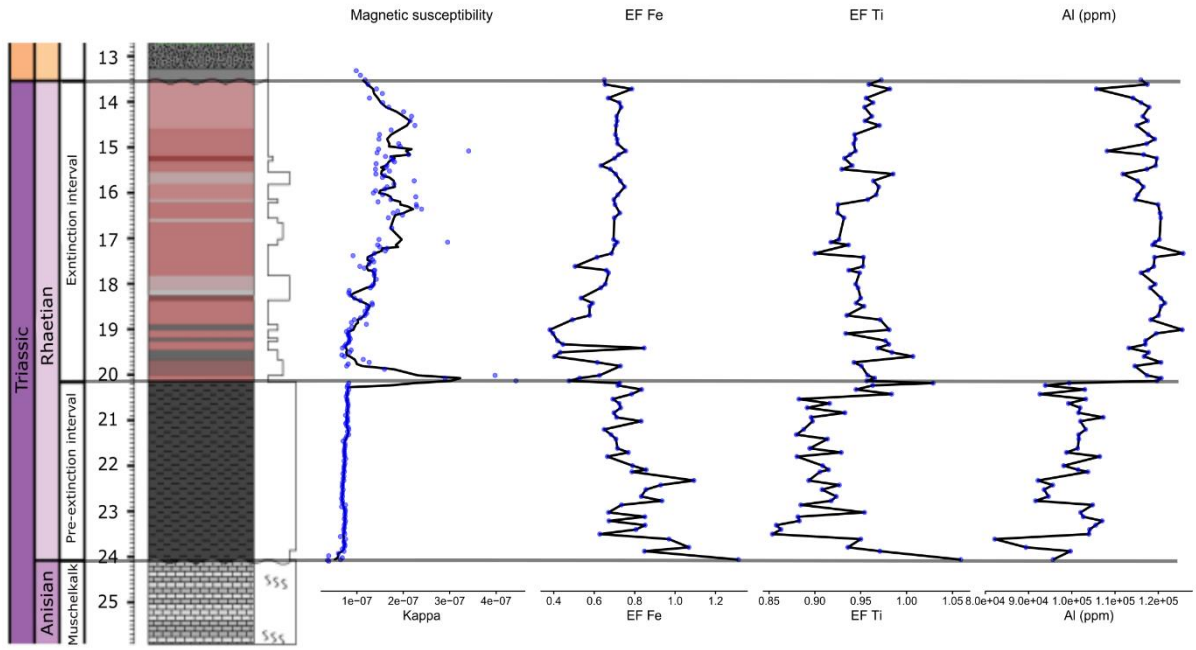

Figure 10. The 4-point moving average kappa (line) and single measurements (blue dots) next to the EF of Fe and Ti and the absolute concentration of Al in ppm.

Palaeoproductivity

Palaeoproductivity is measured via the EF of Ba and P. The enrichment factor of Ba is always below 0.5, and the EF of P is usually below 0.55 (fig. 11). The lowest part of the core is characterised by high enrichment factors of Ba and P, with P constantly increasing until the maximum EF of 0.64 at 23.62 mbs is reached. Both elements show an increasing trend with some variability. The increasing trend persists until the transition. Both elements show a sharp drop at the transition, likely partially caused by the increase in Al (see magnetic susceptibility). After the transition Ba does show some variability but it never recovers to values from before the transition. P generally has a lower EF in the Triletes Beds compared to the Contorta Beds, but has three data points close to 0.5 around 17.11 mbs. The EF of P then drops to around 0.3.

Climatic proxies

The climatic proxies c-value (wetness) and Sr/Cu (dryness) show that the climate changed towards a drier climate in the lowest part of the core, which is especially true for the c-value (fig. 11). Sr/Cu does show some, but not much variability in the Contorta Beds, while the c-value shows a few peaks, but the amplitude of change is rather low. Higher amplitude changes are found after the transition, with Sr/Cu showing a large peak at 8.39 at 19.615

mbs. The large peak in c-value is 1.17 at 19.43 mbs. Two other notable peaks in Sr/Cu are 6.23 and 6.16 at 19.35 and 19.11 mbs respectively. After settling down the c-value does not show any large changes, but Sr/Cu still shows some variability with periods of higher values and sudden drops in values.

Anoxia

V/Cr is used as proxy for anoxia, with an increasing trend towards the maximum of 1.35 at 22.78 mbs (fig. 11). A decreasing trend towards the transition follows. After the transition V/Cr shows some variability and generally a more oxygen-rich environment than in the black shale.

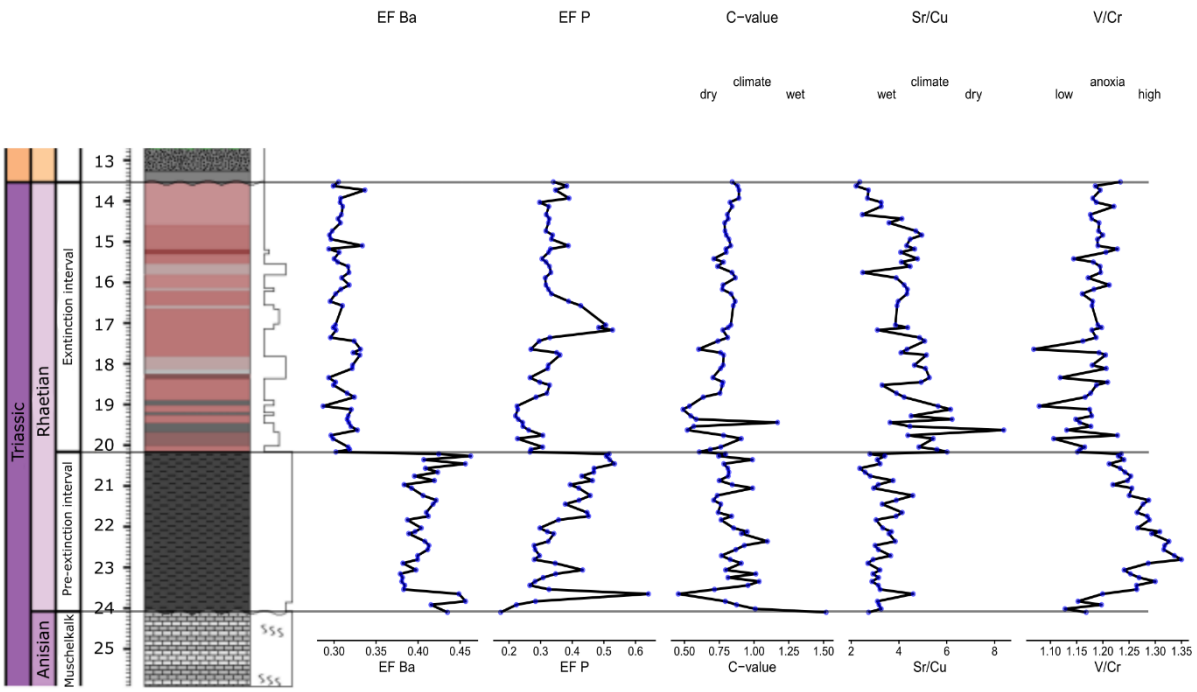

Figure 11. EF of Ba, EF of P, the c-value, Sr/Cu and V/Cr plotted next to the core.

Mercury

Mercury (Hg) increases in the lowest part of the core at the same time that $\delta^{13}C$ decreases (fig. 12). However, Hg shows 7 more spikes, and none of those are accompanied by a significant reduction in $\delta^{13}C$. These Hg spikes happen both in the Contorta and Triletes Beds, and one is just before the transition. Hg shows a lot of variability in the whole core.

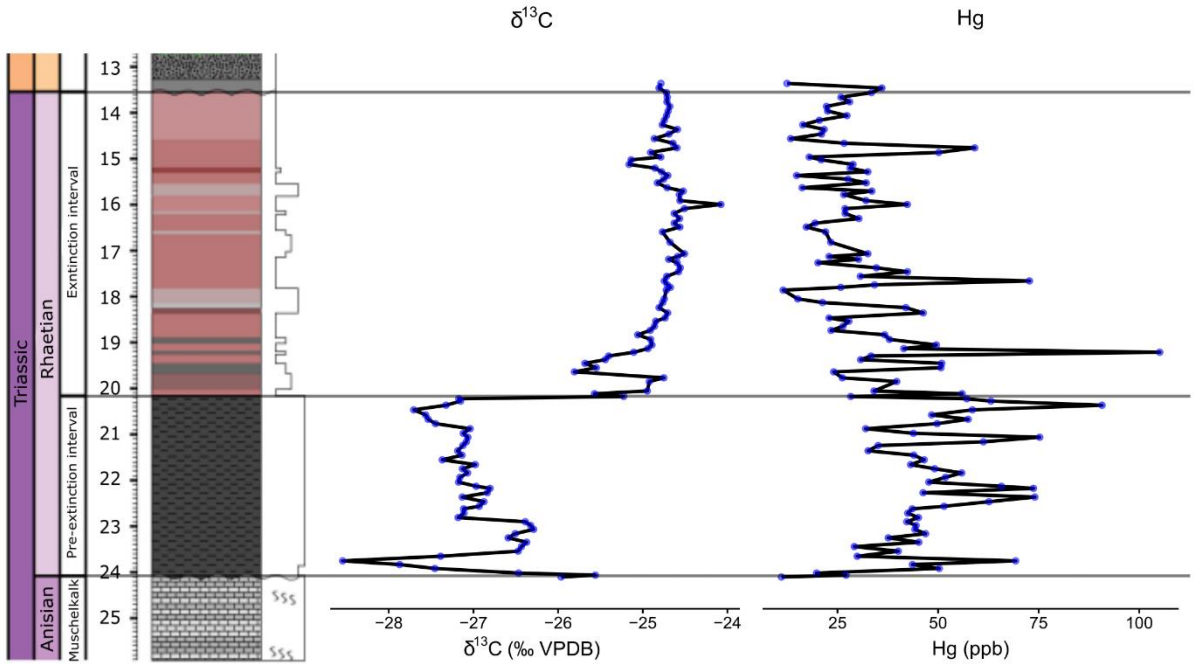

Figure 12. Carbon Isotopes and Mercury concentration in ppb plotted next to the core.

Filtered cyclicity

The TOC in the shale exhibits cyclicity and shows 2 cycles (fig. 13). The peaks in the filter correspond to multiple higher values of TOC, and single data point peaks are not associated with peaks in the filter.

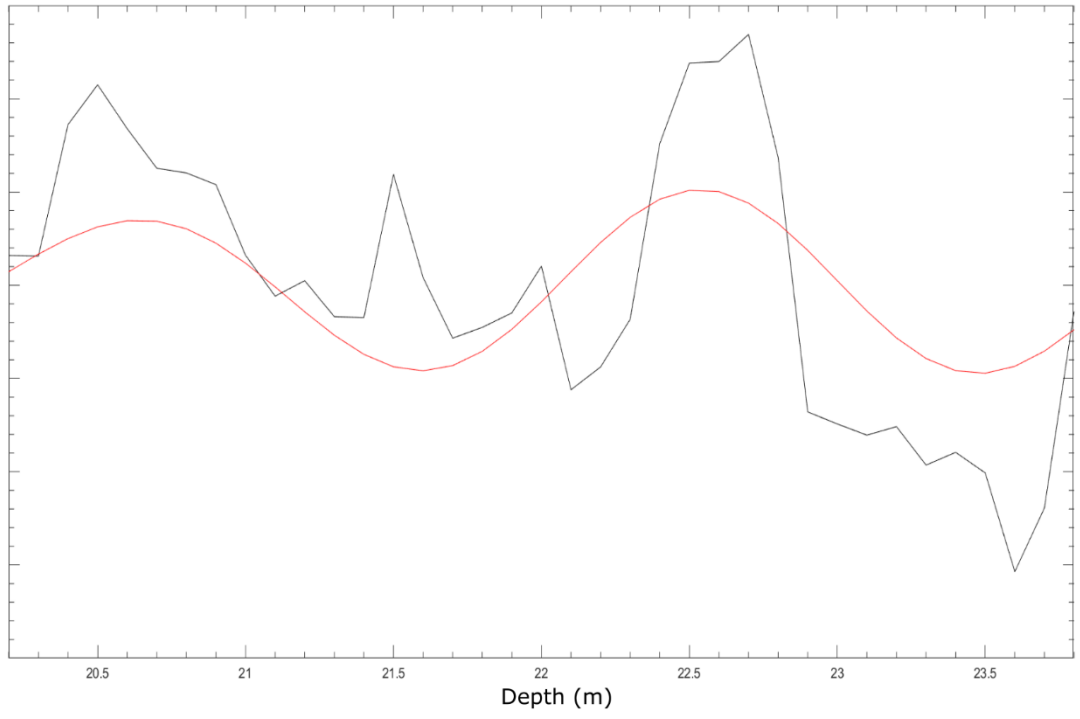

Figure 14. TOC data in the shale in black with a filter between the frequencies 0.43243-0.64865 in red.

The detrended magnetic susceptibility data from the clay is filtered and shows 8 or 9 cycles (fig. 14). Peaks in magnetic susceptibility are associated with peaks in the filter although it seems to be the other way around at 19 mbs and below.

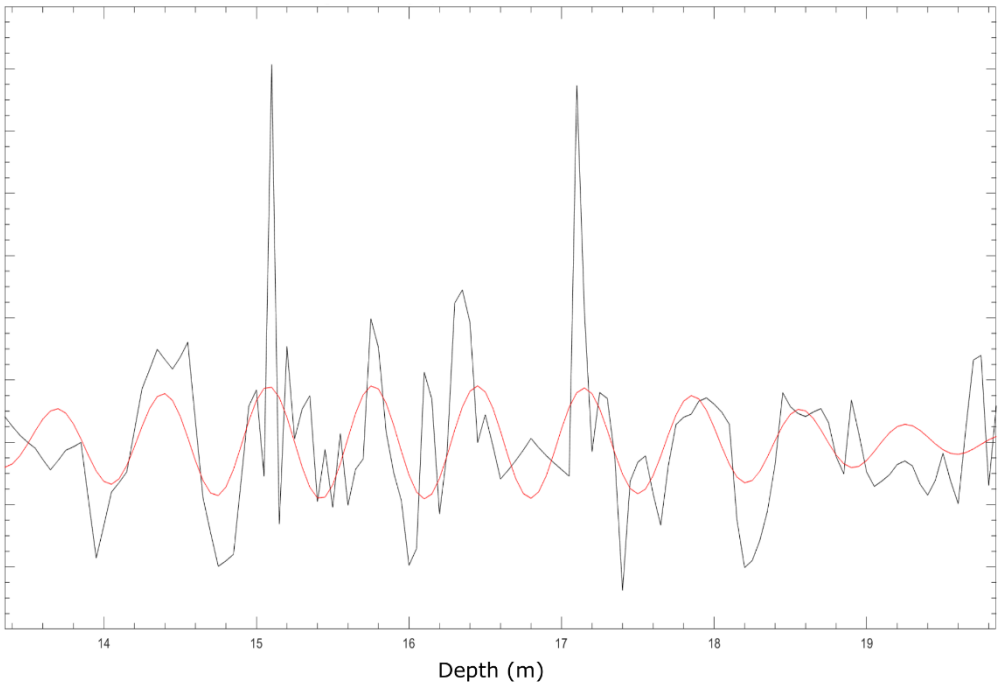

Figure 14. Detrended magnetic susceptibility in the clay (excluding the massive spike at 20.15 mbs) in black and the filter frequency of 1.28-1.59 in red.

Discussion

Timing of the deposition of the Rhaetian part of the core

There is no clear duration of the Rhaetian part of the core. The palynological data firmly establishes the shale and clay to be Rhaetian (Smeets, 2018), and there is no Jurassic sediment. The Marshi CIE indicates that the lowest part of the shale is 201.52 Ma (Lindström et al., 2017). As the TJB (201.36 Ma (Wotzlaw et al., 2014) is not visible in the core, there is less than 165 kyr recorded in the core according to established chronology. This has not taken into account the errors of the dated volcanic rocks. Research into cyclicity in the late Triassic and early Jurassic reveals eccentricity and precession cycles associated with monsoonal activity (Bonis et al., 2010). As nutrients increase with runoff, which is needed for OM production, and nutrients are linked to higher precipitation due to monsoonal activity, TOC values will likely exhibit precession dominated cyclicity. Magnetic susceptibility is influenced by both the 400 kyr and 100 kyr eccentricity cycles and the 20 kyr precession cycle (da Silva et al., 2013). The most likely cycle for the magnetic susceptibility is the 20 kyr cycle, as the eccentricity cycles do not add up to the right amount of time in the extinction interval. Therefore both cycles are presumed precession, which leads to a total duration of the Rhaetian part of the core of 200 kyr, which is in accordance with other studies when taking uncertainties into account. Due to a gradual decline in magnetic susceptibility at the top of the core a precession cycle that is indicated by Acycle might not actually be there. The lowest part of the Triletes Beds also shows a single cycle that does not match well with the data. It might be that there are actually six cycles in the magnetic susceptibility, which would make the total duration of the Rhaetian part of the core 160 kyr.

Palaeoproductivity

The palaeoproductivity proxies EF Ba EF P do not match for both the Contorta and Triletes Beds. Although the two proxies both indicate high productivity in the Contorta Beds the timing of both in- and decreases differ. There are some parts of the core where Ba/Ti decreases while P/Ti increases, around 23 mbs. Vice versa can also be seen at 21.425 mbs. Both proxies do agree that productivity is very high just before the transition. The two palaeoproductivity proxies differ wildly in the Triletes Beds, with EF Ba indicating low productivity and EF P indicating high productivity. Ti/Al vs TOC is used to determine if dilution played a role in the TOC changes in late Triassic shales (Wang et al., 2017). The difference in TOC between the Contorta and Triletes Beds is not caused by dilution, as Ti/Al vs. TOC does not show a large difference between the lithologies. This means that a high palaeoproductivity as indicated by EF P is unlikely. Additionally, the clay corresponds to the extinction interval at other sites, so a low palaeoproductivity is to be expected. However, both Ba and P have their situations where they cannot be used as a palaeoproductivity proxy. Ba is quite mobile and can move via pore waters if there is intense sulfate reduction (Tribovillard

et al., 2006). Although Ba is transported to the sediment via OM, and higher Ba concentration does imply a higher OM production, Ba can move upwards in the sediment during early diagenesis, which can lead to a large deposit of Ba in sediments that are deposited under low OM production conditions. Although the source of P in the water column is mainly OM (Tribovillard et al., 2006), P is cycled back into the water column during anoxic conditions as bacteria form aqueous PO_4^{3-}. As both palaeoproductivity proxies are under-enriched, there remains a possibility that Ba and P are recycled and thus do not show true palaeoproductivity. This is dubious, as changes in the anoxia proxy V/Cr do not reflect changes in the EF of Ba and P.

It is likely that there is a source of P outside of primary productivity, which would explain the mismatch in the proxies in the Triletes Beds.

Magnetic susceptibility

Magnetic susceptibility is dependent on mineral composition (mainly magnetite) and can be influenced by diagenesis and metamorphism, which can lead to remagnetisation and changing of mineralogical composition (da Silva et al., 2013). This makes understanding the magnetic susceptibility signal from the core difficult, as there is no clear way to see if diagenesis played a role. For that the mineralogical composition of the core (especially the clay) has to be studied, to see if there are clay minerals that indicate diagenesis. Clay minerals have a strong magnetic signal, which is the reason that the magnetic susceptibility in the clay is higher than in the shale. Additionally, the concentration of clay minerals in the clay is higher due to less OM in the clay lithology. Furthermore, the main elements that indicate increasing weathering and erosion do not show significant change aside from an increase in Al. Understanding the nature of the peaks in magnetic susceptibility is difficult, but may be related to either a relatively large amount of magnetite in the samples or altering of the clay composition after burial. The extreme peak in magnetic susceptibility at the transition might be due to a different mineralogical composition as there are significant environmental changes at the transition.

Problems with interpreting the transition and the use of carbon data

The lithological change from shale to clay is difficult to interpret by changes in most data, as different lithologies have inherently different compositions, and often different general values for proxies. This is due to a different amount of OM and siliciclastic material, which alters the average composition of the sediment to such a degree that a direct comparison of the two lithologies and the cause of the transition are difficult to interpret. The exception occurs when the elements that influence the data are produced in situ and cannot come from external sources such as erosion and the element used for normalisation does not show a large difference between the two lithologies. As Al has a higher concentration in the clay, a direct comparison of geochemical proxies, such as enrichment factors, between the two

lithologies cannot be made. The difference of amount and type of OM makes a direct comparison of $\delta^{13}C$ impossible. The C/N ratio, considering it is both influenced by the type of OM, with marine organic matter generally having a higher value (Thornton & McManus, 1994), can actually be used across multiple lithologies. The C/N ratio in the shale is much higher than in the clay. This indicates that the shale contains less terrestrial organic matter than the clay, most likely due to a higher palaeoproductivity. It is unclear how much a decrease in the amount of marine OM and an increase in terrestrial OM contribute to the change in C/N, as different types of OM have different C/N ratios, even within terrestrial and marine OM (Thornton & McManus, 1994).

Volcanism

Volcanism leads to the emission of Hg and CO_2, which leads to Hg increasing while $\delta^{13}C$ decreases (Chu et al., 2020; Lindström et al., 2017, 2019). However, the Hg and $\delta^{13}C$ records do not always match (Lindström et al., 2019). However, Hg can also reach the sediment via transport through soils (Zhang & Lindberg, 1999), and via wildfires or baking of organic rich sediment from intrusions (Chu et al., 2020). Hg/TOC is usually used to determine if Hg emissions have increased, as OM can store Hg, so more OM means more Hg in the sediment (Grasby et al., 2013; Lindström et al., 2019). As TOC values in the shale are scattered and there is very little spread in TOC in the clay Hg/TOC cannot be used to determine if Hg emissions are increasing. There is also no correlation between Hg and Al or Ti, so normalising Hg for soil input is not needed. However, this makes it clear that there is no correlation between Hg and the proxies of volcanism and soil input.

Clear evidence for volcanic activity can be seen in the lowest part of the core, where $\delta^{13}C$ values drop and Hg values increase. However, other changes in Hg are not contemporaneous with changes in $\delta^{13}C$, which leads credence to the hypothesis that volcanism is not the only source of Hg in the sediment. There is the possibility that the Hg released by the CAMP is stored in plants and soils and later transported to the sea.

Environmental conditions

During the Rhaetian a large scale regression is followed by a transgression in the late Triassic. (Hallam & Wignall, 1999). Although there has been no exact dating for these events, late Triassic sediments show evidence for sea level fall, such as fluvial sediments on top of shallow marine sediments. Early Jurassic sediments show a transgression, which is not recorded in the core. As the regression happened around the extinction interval of the Rhaetian, it is likely that the regression is at least partly responsible for the lithological transition.

The limestone is formed in a shallow marine environment. Both the Contorta and Triletes Beds are deposited in a calm environment close to the coast, as the limited palynological data (work in progress) of the core show mainly terrestrial palynomorphs.

The climatic proxies of the c-value and Sr/Cu are mostly in agreement with each other about the climatic changes taking place. Clear to see is the decrease in the lowest part of the Contorta Beds of the c-value, which indicates a drier climate. Although the Sr/Cu proxy does not show such a large change, it still shows that the climate became drier compared to before. This may be an effect of volcanism, as discussed above. Other notable observations are cyclicity in both climatic proxies and large fluctuations in especially the Sr/Cu proxy just after the transition. The cyclicity in the Contorta Beds is more regular in the Sr/Cu than in the c-value, although both show rhythmic alternations. In the Triletes Beds the c-value shows barely any cyclicity, but Sr/Cu shows two periods of higher values and three distinct minima. This is most likely due to Milankovitch cycli, as they impact climate and especially precipitation. The large fluctuations of the Sr/Cu after the transition are largely due to changes in the Cu content of the sediment, which indicates that a single element is responsible for changes in the climatic proxy. As the c-value is reliant on more elements, there is less dependency on variations in single elements and the c-value is thus less prone to show rapid changes. While large changes after a sharp lithological and environmental change are to be expected, the fact that only one of the two climatic proxies show this effect diminishes the likelihood of the Sr/Cu proxy being correct in this regard. What the two climatic proxies do agree on is a clear change to wetter climate at 19.43 mbs. The only notable change at that depth is a slightly elevated value of Hg, which makes interpreting this change in climatic proxies problematic. Without indication from other proxies this spike in wetness cannot be explained.

V/Cr as anoxia proxy is used both for recent (as Cr/V) (Schaller et al., 1997) and Triassic-Jurassic sediments ((Richoz et al., 2012). There does not seem to be a link between anoxia and productivity or climate in the Contorta Beds. The drops in anoxia in the Triletes Beds occur mainly during indications of dry climate. This might be due to a wet climate having more freshwater input into the environment and leading to more stratification and anoxia compared to drier conditions.

To fully understand the changes that took place during the Rhaetian at Winterswijk high resolution palynological research is needed to understand climatic changes on land and if vegetational changes correspond to the data that is shown in this study.

Conclusion

- The Marshi CIE is clearly visible in the core.
- The Marshi CIE happens at the beginning of the extinction.
- Volcanism is clearly the source of the Marshi CIE.
- There is a time lag between the Marshi CIE and the extinction at Winterswijk.
- Hg and $\delta^{13}C$ data do not always occur together to indicate volcanism and large changes associated with volcanism, and as such Hg alone is insufficient to determine if volcanism takes place.
- Milankovitch cycli, especially precession, likely played a role in carbon storage and climate variability.
- Magnetic susceptibility is not influenced by the amount of terrestrial input as indicated by the amount of Fe, Ti or Al.
- Palaeoproductivity elements Ba and P do not agree on the evolution and amount of palaeoproductivity.
- It became dry during the period of volcanism at the lowest part of the core
- Climatic variability is higher for ~1.5 m after the lithological transition
- The climatic proxies only sometimes agree on changing conditions
- V/Cr as anoxia proxy does not seem to be reliant on other factors, although a drier climate does sometimes indicate lower anoxia

References

Bambach, R. K. (2006). Phanerozoic Biodiversity Mass Extinctions. *Annual Review of Earth and Planetary Science*, *34*, 127–155. https://doi.org/10.1146/annurev.earth.33.092203.122654

Bonis, N. R., & Kürschner, W. M. (2012). Vegetation history, diversity patterns, and climate change across the Triassic/Jurassic boundary. *Paleobiology*, *38*(2), 240–264. https://doi.org/10.1666/09071.1

Bonis, N. R., Kürschner, W. M., & Krystyn, L. (2009). A detailed palynological study of the Triassic–Jurassic transition in key sections of the Eiberg Basin (Northern Calcareous Alps, Austria). *Review of Palaeobotany and Palynology*, *156*(3–4), 376–400. https://doi.org/10.1016/J.REVPALBO.2009.04.003

Bonis, N. R., Ruhl, M., & Kürschner, W. M. (2010). Milankovitch-scale palynological turnover across the Triassic-Jurassic transition at St. Audrie's Bay, SW UK. *Journal of the Geological Society*, *167*(5), 877–888. https://doi.org/10.1144/0016-76492009-141

Chu, D., Grasby, S. E., Song, H., Corso, J. D., Wang, Y., Mather, T. A., Wu, Y., Song, H., Shu, W., Tong, J., & Wignall, P. B. (2020). Ecological disturbance in tropical peatlands prior to marine Permian-Triassic mass extinction. *Geology*, *48*(3), 288–292. https://doi.org/10.1130/G46631.1

da Silva, A. C., de Vleeschouwer, D., Boulvain, F., Claeys, P., Fagel, N., Humblet, M., Mabille, C., Michel, J., Sardar Abadi, M., Pas, D., & Dekkers, M. J. (2013). Magnetic susceptibility as a high-resolution correlation tool and as a climatic proxy in Paleozoic rocks – Merits and pitfalls: Examples from the Devonian in Belgium. *Marine and Petroleum Geology*, *46*, 173–189. https://doi.org/10.1016/J.MARPETGEO.2013.06.012

Grasby, S. E., Sanei, H., Beauchamp, B., & Chen, Z. (2013). Mercury deposition through the Permo–Triassic Biotic Crisis. *Chemical Geology*, *351*, 209–216. https://doi.org/10.1016/J.CHEMGEO.2013.05.022

Gravendyck, J., Schobben, M., Bachelier, J. B., & Kürschner, W. M. (2020). Macroecological patterns of the terrestrial vegetation history during the end-Triassic biotic crisis in the central European Basin: A palynological study of the Bonenburg section (NW-Germany) and its supra-regional implications. *Global and Planetary Change*, *194*, 103286. https://doi.org/10.1016/J.GLOPLACHA.2020.103286

Hallam, A., & Wignall, P. B. (1999). Mass extinctions and sea-level changes. *Earth-Science Reviews*, *48*(4), 217–250. https://doi.org/10.1016/S0012-8252(99)00055-0

Heimdal, T. H., Svensen, H. H., Ramezani, J., Iyer, K., Pereira, E., Rodrigues, R., Jones, M. T., & Callegaro, S. (2018). Large-scale sill emplacement in Brazil as a trigger for the end-Triassic crisis. *Scientific Reports 2017 8:1*, *8*(1), 1–12. https://doi.org/10.1038/s41598-017-18629-8

Herngreen, G. F. W., van Konijnenburg-van, J. H. A., Oosterink, H. W., & van der Ham, R. W. J. (2005). Nieuwe geologische, palynologische en paleobotanische gegevens (Muschelkalk, Rhaetien-Lias en Oligoceen) uit de steengroeven van Winterswijk. *Grondboor & Hamer*, *59*(4), 84–97.

Kiessling, W., Aberhan, M., Brenneis, B., & Wagner, P. J. (2007). Extinction trajectories of benthic organisms across the Triassic–Jurassic boundary. *Palaeogeography, Palaeoclimatology, Palaeoecology*, *244*(1–4), 201–222. https://doi.org/10.1016/J.PALAEO.2006.06.029

Lee, J. S., Chon, H. T., Kim, J. S., Kim, K. W., & Moon, H. S. (1998). Enrichment of potentially toxic elements in areas underlain by black shales and slates in Korea. *Environmental Geochemistry and Health*, *20*(3), 135–147. https://doi.org/10.1023/A:1006571223295

Li, M., Hinnov, L., & Kump, L. (2019). Acycle: Time-series analysis software for paleoclimate research and education. *Computers & Geosciences*, *127*, 12–22. https://doi.org/10.1016/J.CAGEO.2019.02.011

Lindström, S. (2016). Palynofloral patterns of terrestrial ecosystem change during the end-Triassic event – a review. *Geological Magazine*, *153*(2), 223–251. https://doi.org/10.1017/S0016756815000552

Lindström, S., Callegaro, S., Davies, J., Tegner, C., van de Schootbrugge, B., Pedersen, G. K., Youbi, N., Sanei, H., & Marzoli, A. (2021). Tracing volcanic emissions from the Central Atlantic Magmatic Province in the sedimentary record. *Earth-Science Reviews*, *212*, 103444. https://doi.org/10.1016/J.EARSCIREV.2020.103444

Lindström, S., Sanei, H., van de Schootbrugge, B., Pedersen, G. K., Lesher, C. E., Tegner, C., Heunisch, C., Dybkjær, K., & Outridge, P. M. (2019). Volcanic mercury and mutagenesis in land plants during the end-Triassic mass extinction. *Science Advances*, *5*(10). https://doi.org/10.1126/SCIADV.AAW4018

Lindström, S., Schootbrugge, B. van de, Dybkjær, K., Pedersen, G. K., Fiebig, J., Nielsen, L. H., & Richoz, S. (2012). No causal link between terrestrial ecosystem change and methane release during the end-Triassic mass extinction. *Geology*, *40*(6), 531–534. https://doi.org/10.1130/G32928.1

Lindström, S., van de Schootbrugge, B., Hansen, K. H., Pedersen, G. K., Alsen, P., Thibault, N., Dybkjær, K., Bjerrum, C. J., & Nielsen, L. H. (2017). A new correlation of Triassic–Jurassic boundary successions in NW Europe, Nevada and Peru, and the Central Atlantic Magmatic Province: A time-line for the end-Triassic mass extinction. *Palaeogeography, Palaeoclimatology, Palaeoecology*, *478*, 80–102. https://doi.org/10.1016/J.PALAEO.2016.12.025

Oosterink, H. W. (1986). *Wetenschappelijke Mededeling van de Koninklijke Nederlandse Natuurhistorie Vereniging, Deel 2; De Trias-periode: geologie, mineralen en fossielen*. Hoogwoud: K.N.N.V.

Peace, A. L., Phethean, J. J. J., Franke, D., Foulger, G. R., Schiffer, C., Welford, J. K., McHone, G., Rocchi, S., Schnabel, M., & Doré, A. G. (2020). A review of Pangaea dispersal and Large Igneous Provinces – In search of a causative mechanism. *Earth-Science Reviews*, *206*, 102902. https://doi.org/10.1016/J.EARSCIREV.2019.102902

Raup, D. M., & Sepkoski, J. J. (1982). Mass Extinctions in the Marine Fossil Record. *Science*, *215*(4539), 1501–1503.

Richoz, S., van de Schootbrugge, B., Pross, J., Püttmann, W., Quan, T. M., Lindström, S., Heunisch, C., Fiebig, J., Maquil, R., Schouten, S., Hauzenberger, C. A., & Wignall, P. B. (2012). Hydrogen sulphide poisoning of shallow seas following the end-Triassic extinction. *Nature Geoscience 2012 5:9*, *5*(9), 662–667. https://doi.org/10.1038/ngeo1539

Ruhl, M., Bonis, N. R., Reichart, G. J., Sinninghe Damsté, J. S., & Kürschner, W. M. (2011). Atmospheric carbon injection linked to end-Triassic mass extinction. *Science*, *333*(6041), 430–434. https://doi.org/10.1126/SCIENCE.1204255

Ruhl, M., Kürschner, W. M., & Krystyn, L. (2009). Triassic-Jurassic organic carbon isotope stratigraphy of key sections in the western Tethys realm (Austria). *Earth and Planetary Science Letters*, *281*(3–4), 169–187. https://doi.org/10.1016/j.epsl.2009.02.020

Schaller, T., Moor, H. C., & Wehrli, B. (1997). Sedimentary profiles of Fe, Mn, V, Cr, As and Mo as indicators of benthic redox conditions in Baldeggersee. *Aquatic Sciences 1997 59:4*, *59*(4), 345–361. https://doi.org/10.1007/BF02522363

Schobben, M., Gravendyck, J., Mangels, F., Struck, U., Bussert, R., Kürschner, W. M., Korn, D., Sander, P. M., & Aberhan, M. (2019). A comparative study of total organic carbon-δ13C signatures in the Triassic-Jurassic transitional beds of the central European basin

and western Tethys shelf seas. *Newsletters on Stratigraphy*, *52*(4), 461–486. https://doi.org/10.1127/NOS/2019/0499

Smeets, M. (2018). *Palynological analysis of the Rhaetian clays in the Sibelco WINT15-02 core (Winterswijk, the Netherlands)* [Unpubl. MSc Thesis].

Thornton, S. F., & McManus, J. (1994). Application of organic carbon and nitrogen stable isotope and C/N ratios as source indicators of organic matter provenance in estuarine systems: Evidence from the tay estuary, Scotland. *Estuarine, Coastal and Shelf Science*, *38*(3), 219–233. https://doi.org/10.1006/ECSS.1994.1015

Tribovillard, N., Algeo, T. J., Lyons, T., & Riboulleau, A. (2006). Trace metals as paleoredox and paleoproductivity proxies: An update. *Chemical Geology*, *232*(1–2), 12–32. https://doi.org/10.1016/J.CHEMGEO.2006.02.012

Turekian, K. K., & Wedephol, K. H. (1961). Distribution of the Elements in Some Major Units of the Earth's Crust. *GSA Bulletin* , *72*, 175–192. https://pubs.geoscienceworld.org/gsa/gsabulletin/article/72/2/175/5262/Distribution-of-the-Elements-in-Some-Major-Units

van de Schootbrugge, B., Richoz, S., Pross, J., Luppold, F. W., Hunze, S., Wonik, T., Blau, J., Meister, C., van der Weijst, C. M. H., Suan, G., Fraguas, A., Fiebig, J., Herrle, J. O., Guex, J., Little, C. T. S., Wignall, P. B., Püttmann, W., & Oschmann, W. (2019). The Schandelah Scientific Drilling Project: A 25-million year record of Early Jurassic palaeo-environmental change from northern Germany. *Newsletters on Stratigraphy*, *52*(3), 249–296. https://doi.org/10.1127/NOS/2018/0259

van de Schootbrugge, B., & Wignall, P. B. (2016). A tale of two extinctions: converging end-Permian and end-Triassic scenarios. *Geological Magazine*, *153*(2), 332–354. https://doi.org/10.1017/S0016756815000643

van Zonneveld, R. J. (2021). *The WINT-UU-21 Scientific Drilling Project: Recording the Rhaetian onset of the Triassic-Jurassic extinction event in the Netherlands* [Unpubl. BSc Thesis].

Wang, C., Wang, Q., Chen, G., He, L., Xu, Y., Chen, L., & Chen, D. (2017). Petrographic and geochemical characteristics of the lacustrine black shales from the Upper Triassic Yanchang Formation of the Ordos Basin, China: Implications for the organic matter accumulation. *Marine and Petroleum Geology*, *86*, 52–65. https://doi.org/10.1016/J.MARPETGEO.2017.05.016

Wotzlaw, J. F., Guex, J., Bartolini, A., Gallet, Y., Krystyn, L., McRoberts, C. A., Taylor, D., Schoene, B., & Schaltegger, U. (2014). Towards accurate numerical calibration of the Late Triassic: High-precision U-Pb geochronology constraints on the duration of the Rhaetian. *Geology*, *42*(7), 571–574. https://doi.org/10.1130/G35612.1

Zhang, H., & Lindberg, S. E. (1999). Processes influencing the emission of mercury from soils: A conceptual model. *Journal of Geophysical Research Atmospheres*, *104*(D17), 21889–21896. https://doi.org/10.1029/1999JD900194